Academic Science Journal

Inhibitive Performance of (GO-WO3) in a polyanthranilic acid - Epoxy Resin Matrix for low-Carbon Steels in Hydrochloric Acid

Wasan Abdulfatah Hussen*, Ahmed Najem Abd, and Abdulwahhab H. Majeed

*Department of Chemistry, College of Science, University of Diyala, Diyala, Iraq

*Scichemms2202@uodiyala.edu.iq

Received: 10 August 2023 **Accepted: 10 September 2023**

DOI: https://dx.doi.org/10.24237/ASJ.02.04.800C

Abstract

In this research, polyanthranilic acid, graphene oxide, and tungsten oxide Nanoparticles were synthesized using a cutting-edge preparation technique. In the next step, GO-10%WO3, nanocomposite was prepared by adding the 10% of the weight ratio of tungsten oxide. In another step, a solution of polyanthranilic acid was mixed with epoxy resin to prepare the mother solution (Epoxy-PANA), GO(0.05 g) /Epoxy-PANA, (GO-10%WO3) (0.05 g)/Epoxy-PANA) were prepared, in addition to (Epoxy-PANA). The materials that were readied for analysis underwent characterization utilizing FTIR, XRD, EDX and SEM. In the end, it's use as anti-corrosion materials by coating it with low carbon steel. It was found that Inhibition efficiency increased by adding tungsten oxide nanoparticles to the coatings. On the contrary, the rate of corrosion is diminished by adding tungsten. Moreover, it was found that adding the percentage 10% of WO3 leads to affects the concepts of activation energy (Ea), enthalpy (ΔH) and entropy (ΔS) are important in this context.

Key words: GO, WO3, Nanocomposite, Corrosion inhibition.

الأداء المثبط لـ (GO-WO3) في حمض البولي أنثرانيليك ـ مصفوفة راتنجات الايبوكسي للفولاذ منخفض الكربون في حمض الهيدروكلوريك

وسن عبد الفتاح حسين و احمد نجم عبد و عبد الوهاب حميد مجيد

قسم علوم الكيمياء – كلية العلوم – جامعة ديالى

Academic Science Journal

الخلاصة

في هذه الدراسة، تم تعزيز تثبيط التآكل للفولاذ منخفض الكربون من خلال إدراج المركبات النانوية لأكسيد الجرافين والتنغستن داخل مصفوفة راتنجات الإيبوكسي. ولتحقيق ذلك، تم تصنيع البولي (حمض الأنثرانيليك) وأكسيد الجرافين وجسيمات أكسيد التنغستن النانوية ودمجها لإنشاء المركب النانوي (GO -10%WO3)، حيث تم تضمين 10٪ من نسبة وزن أكسيد التنغستن. تم بعد ذلك خلط محلول بولي (حمض أنثرانيليك) مع راتنج الإيبوكسي لإنشاء المحلول الأصلي (إيبوكسي / بانا)، والذي تم استخدامه لإنتاج الطلاءات البوليمرية ((GO/Epoxy-PANA،

GO -10% WO3/ Epoxy-PANA،و (Epoxy-PANA). تم تحليل المواد المعدة بدقة من خلال FTIR و XRD و EDX و SEM. في النهاية، تم تطبيق الطلاء على الفولاذ منخفض الكربون لتقييم فعاليته كمواد مقاومة للتآكل. أشارت النتائج إلى أن إدراج جزيئات أكسيد التنغستن النانوية أدى إلى تحسين كفاءة تثبيط الطلاء، مع تقليل معدل التآكل في نفس الوقت. بالإضافة إلى ذلك، تمت دراسة تأثير تضمين 10٪ WO3 على طاقة التنشيط (Ea)، والمحتوى الحراري (ΔH)، والإنتروبيا (ΔS).

الكلمات المفتاحية : GO، WO ، المركبات النانوية، تثبيط التآكل.

Introduction

The inevitability of corrosion natural process, poses a significant challenge to industries and infrastructures worldwide. The degradation of materials, metals, such as low carbon steel, are of particular interest. Due to the corrosive effects of environmental factors such as moisture, salt, and chemical agents, results in substantial economic losses and safety concerns. As a result, the quest for efficient and sustainable corrosion inhibition strategies has led to the exploration of advanced materials and innovative techniques [1-5]. Graphene oxide (GO) has emerged as a prominent material in research in recent years, as a remarkable nanomaterial with immense potential to revolutionize the field of corrosion inhibition. Graphene oxide, a derivative of graphene, the material displays a 2D configuration composed of carbon atoms arranged in a hexagonal pattern. Its unique properties, including high surface area, exceptional mechanical strength, and intriguing electronic structure, have propelled GO into the forefront of materials research. Beyond its celebrated applications in electronics, energy storage, and biomedicine, the corrosion inhibition prowess of GO has garnered significant attention [6 -7].

The incorporation metal oxide particles, including WO3, TiO2, MnO2, and ZnO, among others, are being studied.into graphene oxide matrices presents a promising strategy for augmenting

the corrosion inhibition capabilities of materials. This innovative approach leverages a synergistic blend of physicochemical and electrochemical mechanisms, enabling these oxide particles to provide robust protection to metals against corrosive processes [8-12]. By integrating metal oxide particles within graphene oxide frameworks, a multifaceted defense mechanism is established. The physicochemical attributes of the metal oxide particles contribute to a reinforced barrier effect, the prevention of corrosive agents from reaching the metal surface. This barrier, formed through interfacial interactions and adsorption phenomena, minimizes the initiation and progression of corrosion [13-14]. Furthermore, the presence of metal oxide particles within the graphene oxide matrix introduces enhanced stability and mechanical reinforcement. This not only bolsters the structural integrity of the composite material but also ensures prolonged and sustained corrosion protection by maintaining the barrier effectiveness over time [15-16].

On the other hand, conductive polymers have recently gained significant attention from researchers as effective anti-corrosion agents are preferred for their environmental stability, Low cost and ease of use for corrosion control [17]. These polymers feature elongated carbon chains that effectively cover extensive areas of corroded metal surfaces upon adsorption, offering protection [18]. An important advantage of conductive polymers and their nanocomposites lies in their affordability relative to alternative coatings. Furthermore, they serve as both physical and electronic barriers, enhancing the safeguarding effects beyond those provided by materials acting solely as physical barriers [19]. Polyaniline (PANI) and its derivatives such as poly anthranilic acid, among the investigated conductive polymers, hold particular significance due to their economical nature, exceptional environmental stability, and adeptness for controlled charge transfers [20].

In the similar studies, Zhang et al [21]. Produced a composite material consisting of PANI-graphene-TiO2, which they applied uniformlyon to 304 stainless steel to combat corrosion. Their findings indicate that this ternary composite display a more robust response to the comparison is made between visible light and pure TiO2. Additionally, the composite exhibits marked improvement in its photoelectrochemical performance when subjected to visible light irradiation. Chen et al. [16] a ternary nanocomposite, TiO2/Graphene oxide/Polyaniline

(TiO2/GO/PANI), was created via in situ oxidation. This composite was used as a filler in epoxy resin, forming TiO2/GO/PANI/EP. This innovative approach led to the creation of a dual-purpose in situ protective coating that effectively enhanced the authors conducted research on safeguarding Q235 carbon steel against corrosion[22].Synthesized a nanocomposite coating by combining tungsten trioxide (WO3) nanoparticles with epoxy resin. The resulting coating was then applied to brass samples to assess its effectiveness in providing corrosion protection, particularly in stressed [22].

The study yielded results indicating a reduction in corrosion rate of low-carbon steel upon coating with polymeric nanocomposites. Specifically, when coated with polymer-epoxy and hardener at a ratio of 1:1, initial corrosion rates decreased, followed by further reduction upon addition of multi-walled carbon nanotube - oxidizer to the mixture. Subsequently, corrosion rate decreased even more upon introduction of tungsten oxide, with careful attention given to proportions. Notably, corrosion inhibition efficiency increased until reaching 99.24%. Additionally, an increase in tungsten oxide percentage was observed to increase electrical conductivity.

Experimental

Chemicals and Instrumentations

The chemicals as well as the solvents were acquired directly from the source. companies such as Riedel-de haën, SDH, and Sigma-Aldrich. They were utilized in their as-received state without any purification or modification. In order to analyze the materials prepared, FTIR was conducted by a (Perkin Elmer FT-IR 65) instrument. X-ray diffraction (XRD) analysis was successfully conducted by means of a Shimadzu XRD-6000 apparatus employing Cu Kα radiation (wavelength of 1.5406 Å). The TESCAN MAIA3 scanning electron microscope was utilized to investigate the surface characteristics of the specimens.

Methods:

Preparation of graphene oxide (GO) nanosheets:

GO nanosheets in the present study employed a modified Hummer methodology utilizing graphite as the source material. In a 250 ml conical flask that was cooled in an ice bath, a mixture of 0.5g of powder graphite, and 1g (0.0135 mol) of sodium nitrate (NaNO3) was vigorously

stirred in the presence of 23 ml of concentrated H2SO4 for a duration of 20 minutes. Subsequently, 3.0 g of potassium permanganate (KMnO4) was gradually added to the mixture while maintaining the temperature between 0-5°C and stirring rapidly. The mixture was moderately stirred for one hour. Thereafter, 50.0 ml of H2O was slowly added to the suspension under strong stirring. To reduce the permanganate concentration, 150.0 ml of warm distilled water was added, and 5.0 ml of 30% hydrogen peroxide was utilized to dissolve manganese ions. The final suspension was filtered, repeatedly washed with warm distilled water, and then subjected to ultrasonic treatment for GO nanosheets exfoliation. The nanosheets obtained were subsequently dried at 90°C in an oven for 24 hours to yield GO powder[23-24].

Preparation of poly (anthranilic acid) (PANA):

PANA was produced by polymerizing anthranilic acid with (6 g) of ammonium persulfate ($(NH_4)_2S_2O_8$) (APS) in a room-temperature using aqueous solution containing acetic acid. Initially, 2.05 g of anthranilic acid was added to 50 ml of acetic acid (1 M) while stirring. APS, dissolved in 50 mL of distilled water was gradually introduced into the monomer solution in a dropwise manner. Subsequently, the resulting mixture was subjected to stirring at room temperature for a duration of 24 hours. Upon completion of the addition, the obtained product was subjected to filtration followed by multiple washes with 1 M acetic acid, and final rinsing with deionized water to eliminate any residual acetic acid. The resultant precipitate was allowed to air dry for a period of 48 hours at ambient conditions [25-26].

Preparation of Tungsten Oxide (WO3) Nanoparticles:

100 ml of W stock solutions with 5ml of ethylene glycol were irradiated using manual irradiation system for 2h separately(A mercury lamp source is used, placed inside a quartz tube, in order to isolate all wavelengths except ultraviolet rays, which are considered the appropriate rays for the reaction to occur). Green precipitate was formed, then, it was washed by deionized water and isolated by decantation process. The precipitate was dried in the oven at 80 oC for 5h. After that, the precipitate calcined at 400 oC for 3h. Finally, light green precipitate was formed.

Preparation of graphene oxide-tungsten oxide (GO-10%WO3) nanocomposite:

To synthesize the binary nanocomposite GO-10%WO3, a quantity of 0.45 g of graphene oxide (GO) was introduced to 20 ml of absolute ethanol and subjected to suspension via ultrasound for a duration of 10 minutes. Subsequently, a quantity of 0.05 g of tungsten oxide (WO3) was incorporated into the graphene oxide suspension and the resulting mixture was subjected to further ultrasonic waves for a duration of 20 minutes. Following this, the mixture was allowed to stir for 30 minutes. The resultant product was dried at 70°C for 24 hours to yield the GO-10%WO3 nanocomposite.

Preparation of Epoxy-Poly (Anthranilic Acid) (PANA) Polymer composite:

The preparation of the mother solution, Epoxy-PANA, involved the direct combination of a poly anthranilic acid solution with epoxy resin. Initially, 0.5 g of poly (anthranilic acid) (PANA) was dissolved in 30 ml of absolute ethanol and left to stir for 30 minutes, until complete dissolution was achieved. Subsequently, 30 ml of (1:1) Epoxy resin(on the candidate list published by the

European Chemicals Agency in concentrations above (0.01 %)w/w, was gradually added to the polymeric solution while vigorously stirring, until a thorough mixing was attained. Further stirring for an hour ensured the formation of a homogenous polymeric solution, comprising of epoxy and poly (anthranilic acid) (Epoxy-PANA).

Preparation of polymeric coatings:

The polymeric nanocomposites used for the process of coating the low carbon steel piece were prepared in order to protect it from corrosion. The mother solution is the first polymeric compound used to paint the steel piece. Whereas, in the second polymer composite, it was prepared by adding 0.05 g of graphene oxide to 10 ml of the mother solution, then the solution was suspended using ultrasound waves until the solution was homogeneous, subsequently, 5 ml of hardening agent was incorporated into the concocted amalgam, which was subsequently subjected to suspension for a duration of 30 minutes. The resultant mixture was employed to coat the steel component. Ultimately, the third polymeric compound was formulated. In order to achieve this, 0.05 g of GO-10%WO3 was introduced into 10 ml of the mother solution. The solution was then subjected to ultrasound treatment until homogeneity was attained.

Subsequently, 5 ml of the hardening agent was introduced into the prepared mixture, which was then suspended for a period of time. Following a duration of 30 minutes, the mixture was utilized to coat the steel piece.

Measurement of Weight Loss

The corrosion rate values were determined utilizing the weight-loss approach, employing equation (1). This non-electrochemical method is utilized to determine the corrosion rate and inhibitor efficiency, and yields more reliable outcomes than electrochemical methods, as it addresses experimental circumstances in a more realistic manner [27-28].

To determine the weight loss of pre-cleaned and completely dried steel test samples, the samples were initially weighed, and subsequently immersed in a beaker containing 100 ml of 1 M HCl for 3 h, both in the presence and absence of the inhibitor (Epoxy-PANA), (GO/ Epoxy-PANA), (GO –10% WO3/ Epoxy-PANA) corrosion rates and inhibition efficiency were investigated at diverse temperatures in 1 M HCl. Conversely, the impact of various temperatures (10,20, 30,40, 50)℃ on the aforementioned factors was explored. The outcomes were compiled in Tables (1). The corrosion rates (CR) pertaining to low carbon steel were computed through weight reduction utilizing the formula presented in equation (1) [29].

$$C_R = \frac{\Delta W}{A \times t} \times 240000 \quad \ldots\ldots\ldots\ldots\ldots\ldots\ldots\ldots\ldots\ldots \quad (1)$$

Where: The weight loss (g) is represented by ΔW, while surface area (m2) is denoted as, and the time of exposure (day) is indicated as t. Where corrosion rates are given in units of g/m2.d which is denoted by (gmd).

Where: To ascertain the inhibition efficiency (IE), the subsequent formula, which may be articulated in the form of equation (2), was employed [30].

$$IE\% = \frac{W_{uninh} - W_{inh}}{W_{uninh}} * 100 \quad \ldots\ldots\ldots\ldots\ldots\ldots\ldots\ldots\ldots\ldots \quad (2)$$

Where: (IE%) represents the efficiency of inhibition, (W uninh) is the weight in the presence of the inhibitor, and The weight without the inhibitor, denoted as (W inh), was recorded as part of the experimental results presented in Tables (2). Analysis of the data revealed that the corrosion rate was positively correlated with temperature, but inversely correlated with inhibitor

concentration. Moreover, the introduction of a polymeric nanocomposite inhibitor led to an increase in inhibition efficiency.

Table 1: The effect of temperature on the corrosion rate of low-carbon steel

T ℃	Corrosion With rate out inhibitor(gmd)	(GO / Epoxy-PANA) gmd	(GO –10% WO3/ Epoxy-PANA) gmd
10	g/ h . m2	73.44723	83.05723
20	102.7716	125.5455	60.68402
30	187.5916	171.757	78.27947
40	732.2837	146.1481	76.6149
50	3444.6	178.1289	79.74333

Table (2): Effect of temperature on the present study investigates the inhibition efficiency (IE%) of corrosion for low carbon steels in a 1M hydrochloric acid solution in the presence of various corrosion inhibitors, namely (Epoxy-PANA), (GO/Epoxy-PANA), and (GO –10% WO3/ Epoxy-PANA).

T	(Epoxy-PANA)	(GO / Epoxy-PANA)	(GO –10% WO3/ Epoxy-PANA)
℃	IE%	IE%	IE%
10	42.25855	28.53355	19.18272
20	60.32289	33.07508	67.65099
30	91.00164	76.54502	89.31023
40	98.74503	95.75718	97.7758
50	98.86081	97.65207	98.9489

Result and Discussion

FTIR:

The GO FTIR spectrum was presented in Figure (1), revealing characteristic peaks at 3426, 1720, 1628, and 1058 cm-1, which can be allocated to ν(O-H), ν(C=O), ν(C=C) in unoxidized graphite, and ν(C-O), respectively [31]. As presented in Figure (1), the FTIR spectrum of PANA exhibits distinct bands at 3370, 3210, 1690, 1607, 1517, and 1244 cm–1, which can be recognized to ν(O-H), ν(N-H), ν(C=O), ν(C=C quinoid), ν(C=C benzenoid), and ν(C-H), respectively. It is noteworthy that these bands have been previously reported [25-32].

Academic Science Journal

The FTIR spectra of investigated powder specimens of WO3 are depicted in Figure (1). Two prominent peaks are observed at approximately 820 and 750 cm-1, representing the stretching mode of (O–W–O). Additionally, distinctive bands are observed near 3460 and 1518 cm-1, corresponding to the H–O stretching and bending modes of water [33,34].

On the one hand, Figure (1) also shows the FTIR spectrum of GO-10%WO3 nanocomposites. It is noted from the FTIR spectrum of GO-10%WO3 that bands appear due to graphene oxide at 3411, 1719 and 1621 cm-1, which are due to the vibrations of the hydroxyl group (O-H), carbonyl group (O=C) and (C=C) group, respectively. As for the remaining bands, which are centered at 820 and 743 cm-1, they represent the (O-W-O) stretching vibrations of tungsten oxide.

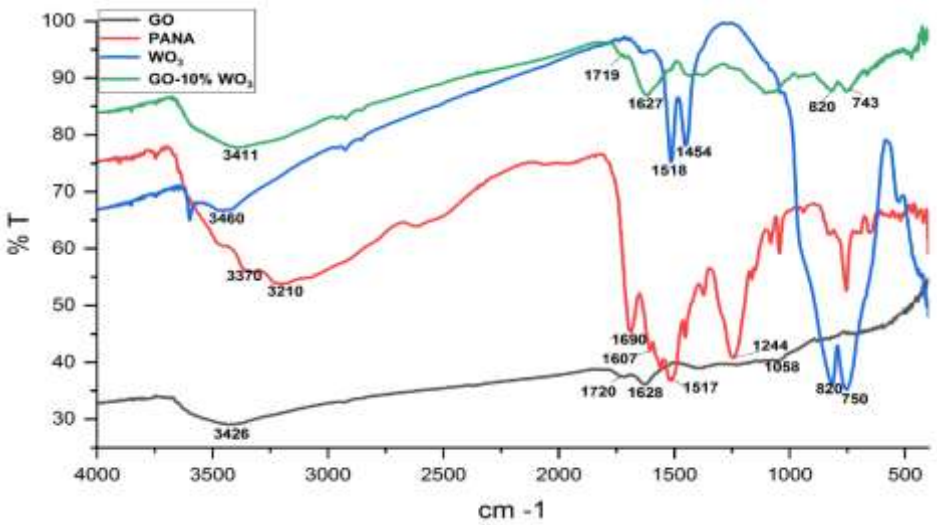

Figure 1: FTIR of GO, PANA, WO3 and GO-10% WO3.

XRD:

In Figure 2, the XRD spectra of Gt and GO are presented. The XRD analysis of graphite (Figure 2.a) is crucial for discerning structural changes in the prepared graphitic materials. The XRD pattern of graphite reveals two distinct peaks at 2θ angles of 26.51° and 54.63°, corresponding to interlayer distances of 3.365 Å and 1.687 Å, respectively [35].

Conversely, the XRD analysis of GO (Figure 2.b) demonstrates a notable peak at 2θ = 10.111°, signifying an interlayer spacing of 8.735 Å. This peak is linked to the formation of oxygenic groups on the surfaces of sheet (-OH, -COOH, -C=O, and –C-O-C-) as a consequence of the

oxidation procedure. Furthermore, GO exhibits a peak at 2θ = 23.941°, arising from the incomplete exfoliation of the starting material (graphite) [36].

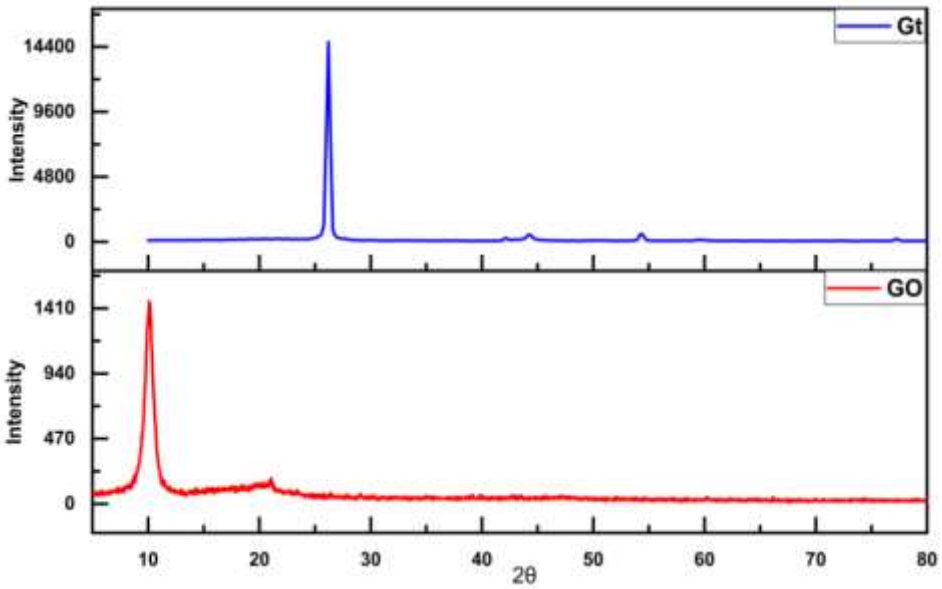

Figure 2: XRD of graphite and graphene oxide.

Figure 3 displays the XRD analysis of the prepared WO3 and the(GO-10%WO3) nanocomposites. The diffractogram of WO3 nanoparticles exhibits distinct peaks at 23.225°, 23.775°, 24.425°, 28.925°, 34.275°, and 41.875°, conforming to the (002), (020), (200), (112), (202), and (222) lattice planes of WO3, respectively. By comparing the diffractogram with the standard patternscard found in (JCPDS no. 00-043-1035), it is confirmed that the nanoparticles possess the characteristic monoclinic structure of tungsten trioxide (WO3) [37-41]. In addition, the same figure (3) shows the XRD analysis of GO-10%WO3 nanocomposites. It is noted from the figure that distinct peaks appear within the range 5-80 o. The peak centered at locations (7.6322) is due to graphene oxide, while the other peaks are due to tungsten oxide, Because the ionic diameter of the tungsten oxide ions (+6) is smaller than the diameter of the carbon molecules in graphene oxide, therefore, during their interaction the shifted at the peaks of the grapheme.The appearance of the peaks of graphene oxide and the peaks of tungsten oxide indicates the success of the interaction between graphene oxide and tungsten oxide.

Academic Science Journal

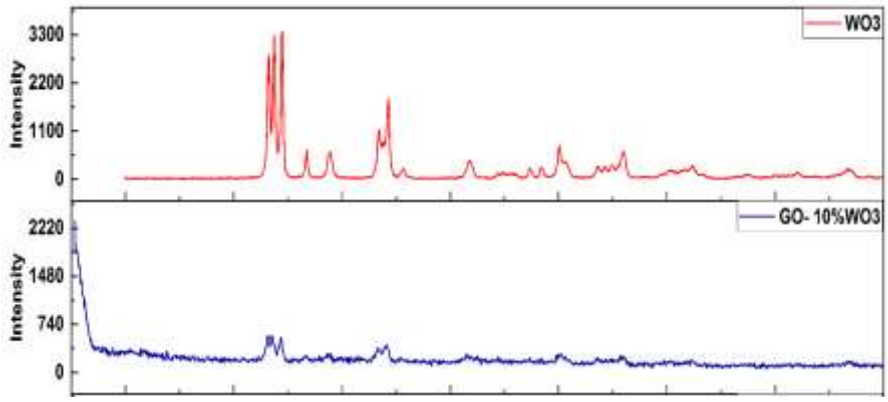

Figure 3: XRD of WO3, GO-10% WO3 nanostructures.

EDX:

Figure 4 (a-d) displays the EDX spectra of Gt (graphite), GO (graphene oxide), WO3 and GO-10%WO3, respectively. The EDX spectrum of Gt (figure 4. a) indicates a 100% weight ratio of carbon peak at Kα = 0.27 keV [42-43]. On the other hand, the EDX analysis of GO (figure 4. b) reveals a composition of GO nanosheets with a 52.21% wt. of carbon signal at Kα = 0.27 keV and a 47.79% wt. of oxygen signal at Kα = 0.50 keV. The higher oxygen content in GO compared to Gt is attributed to the oxidation methods involving a good oxidants such as KMnO4, NaNO3, and H2SO4 [42-44].

In the case of pure WO3(figure 4. c), the EDX spectrum will primarily show peaks corresponding to oxygen (O) at Kα= 0.50 keV, with 35.64% wt. of WO3 and the peaks of tungsten (W) in a different location with 64.36 of weight ratio of WO3. The intensities of these peaks will provide information about the relative abundance of each element in the sample. Some other unmarked peaks are also observed, which result from preparing the sample for examination in the device. Ideally, the spectrum should only exhibit peaks for W and O, confirming the sample's purity [45-47].

Furthermore, the EDX analysis of GO-10%WO3 shown in figure (4-d). The analysis indicates the elemental composition of the graphene oxide (GO) samples doped with 10% weight of tungsten oxide (WO3). The analysis shows the presence of a peak of carbon, which belongs to GO, and peaks of tungsten, which represent WO3. It is also noted that there is a peak of oxygen,

which represents GO and WO3. The presence of all these peaks point to the successful interaction between graphene oxide and tungsten oxide.

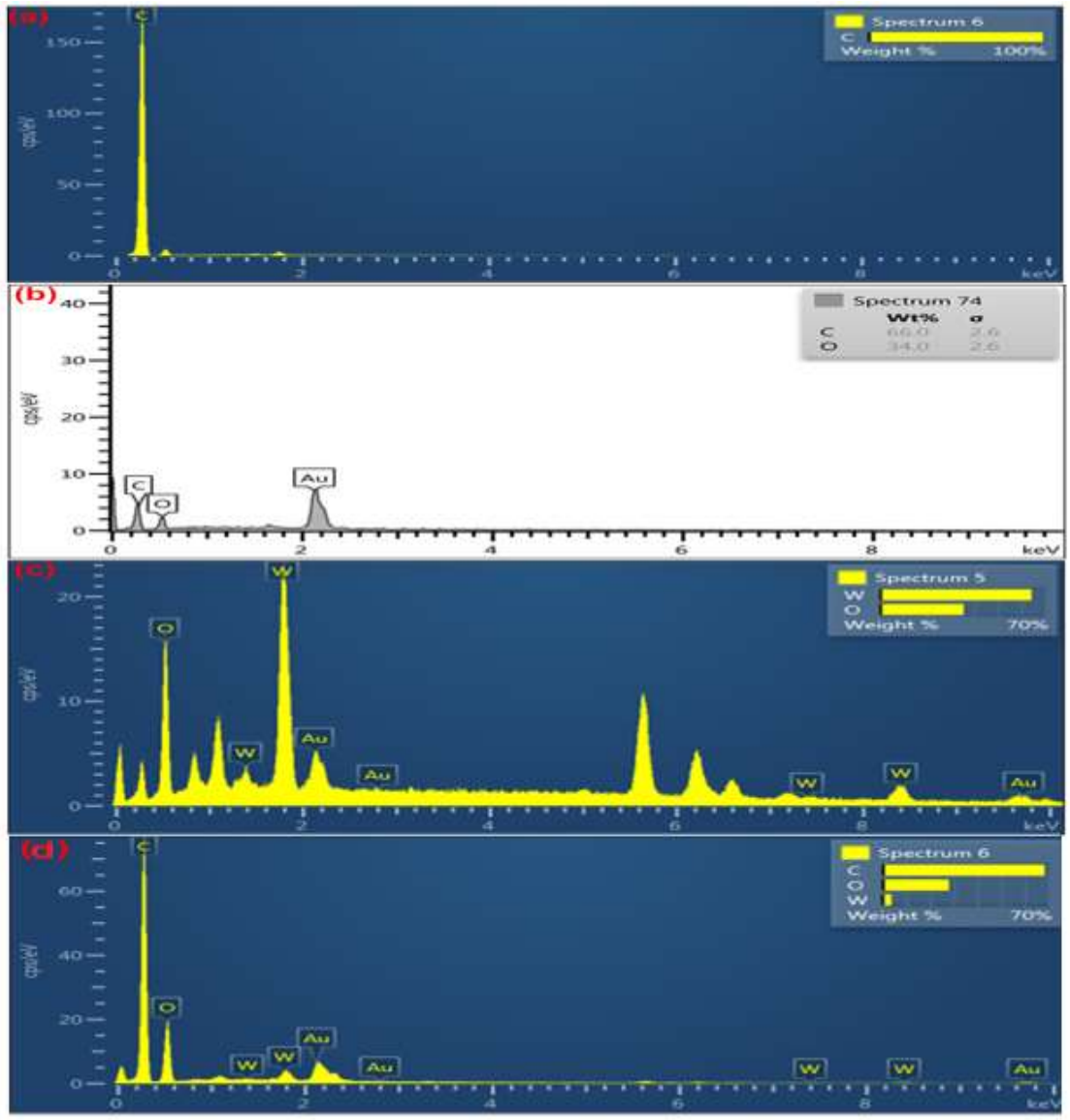

Figure 4: EDX of (a) Gt, (b) GO, (c) WO3, and (d) GO-10% WO3.

Study morphology by FE-SEM:

The scanning electron microscope (FE-SEM) is a sophisticated imaging tool extensively employed for examining the surface topography and dimensions of various samples at a nanoscale resolution. This technology finds widespread application in diverse scientific fields,

including materials science, nanotechnology, biology, geology, and more, aiding in comprehensive material analysis and research [48-50].

Figure (5(a-h)) shows the FE-SEM examination of graphite (Gt), graphene oxide (GO) nanosheets tungsten oxide (WO3) and GO-10%WO3 nanocomposites.The (FE-SEM) examination of the graphite shown in the figure (5.a) shows that it appears as a large block of graphite in the form of stacked sheets. Also, this large composition contains some deformations and small parts above the plates, and these results from the graphite grinding process.

Figure (5.b-d) presents the FE-SEM examination of graphene oxide nanosheets. It is noted from the figure that thin, smooth sheets appear that do not contain distortions and defects on the surface of the sheet, and this indicates the success of the used preparation method. It is also noted that there are some folds on the surface of the plate, and this is a result of the twisting of the plate itself or the accumulation of one part of the plate on another part of it, to be in this structure.

Figure (5.e,f) shows the FE-SEM examination of tungsten oxide (WO3) nanoparticles. The figure shows that the WO3 nanoparticles have irregular structures and different diameters starting from 35 nm. It is also noted that there are some clusters of these particles resulting from the accumulation of some of them to form large masses.

And Figure (5. g, h) shows the (FE-SEM) examination of the GO-10%WO3 nanocomposite. It can be seen from the figure that the WO3 particles are uniformly. It is noticeable in this figure that the WO3 particles are spread on a regular basis on the graphene oxide plates, and this proves that the process of preparing this nanocomposite was successful, as indicated in the previous diagnostic figures.

Academic Science Journal

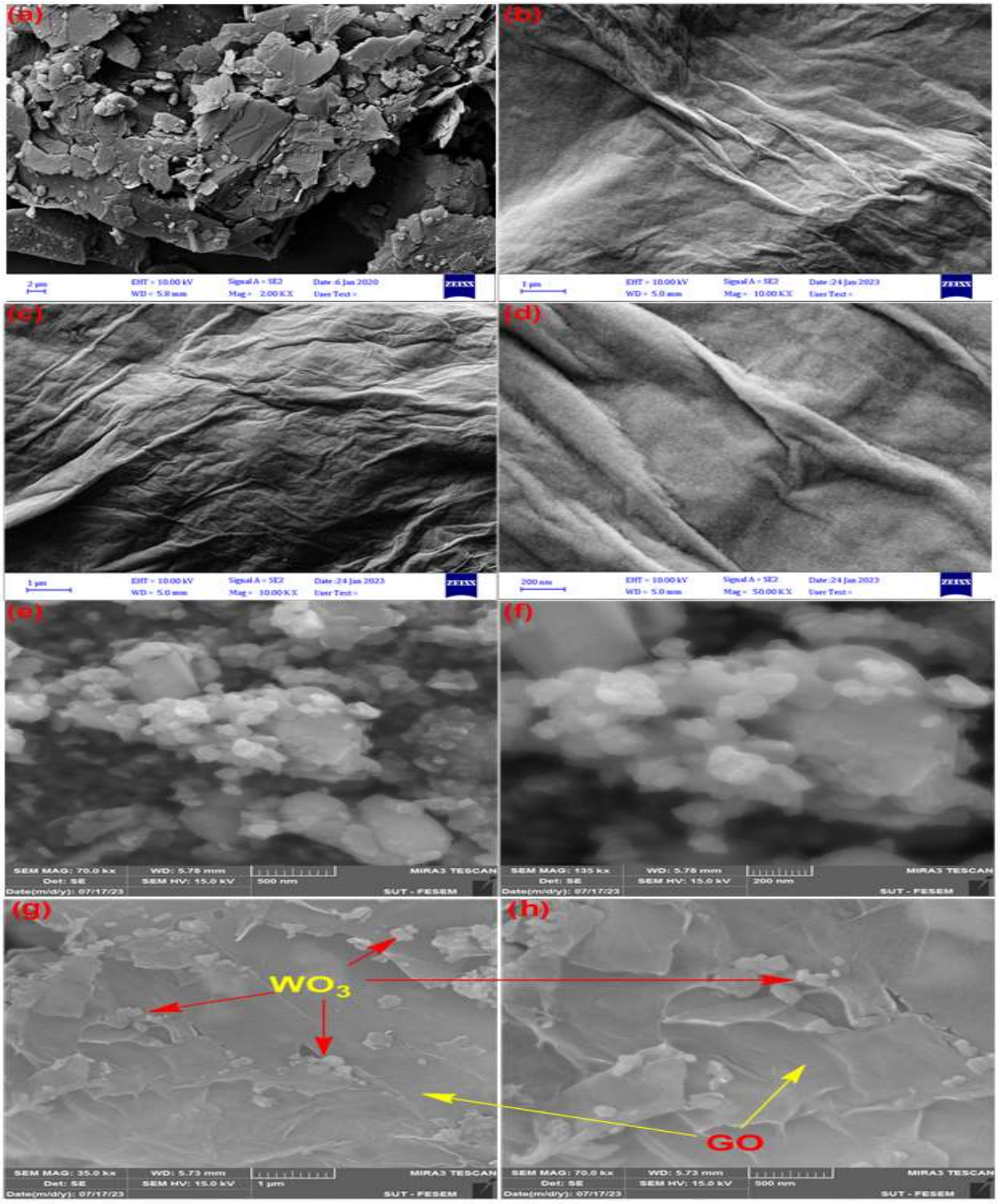

Figure 5: FE-SEM of (a) Gt, (b to d) GO, (e, f) WO3, and (g, h) GO-10% WO3.

Academic Science Journal

Figure 6 represents an FE-SEM examination of a piece of low-carbon steel coated with (Epoxy-PANA) after immersing it in (1M) HCL acid for (3 hours) and at (50 °C). It is noted from the figure that there is a small amount of deformation resulting from the treatment of acid with the coated steel piece.The acid did not affect much the coated steel due to the resistance of the polymer to the acid and its interaction with the acid and the current investigation has established that the creation of a protective layer effectively inhibits corrosion of low carbon steel. As evidenced by the results of our study, the impact of acid, temperature, and time was minimal, as little corrosion was observed from the figure. These findings highlight the efficacy of protective coatings in preventing corrosion, where the corrosion percentage was (86.42608) and the inhibition efficiency was (98.8608%).

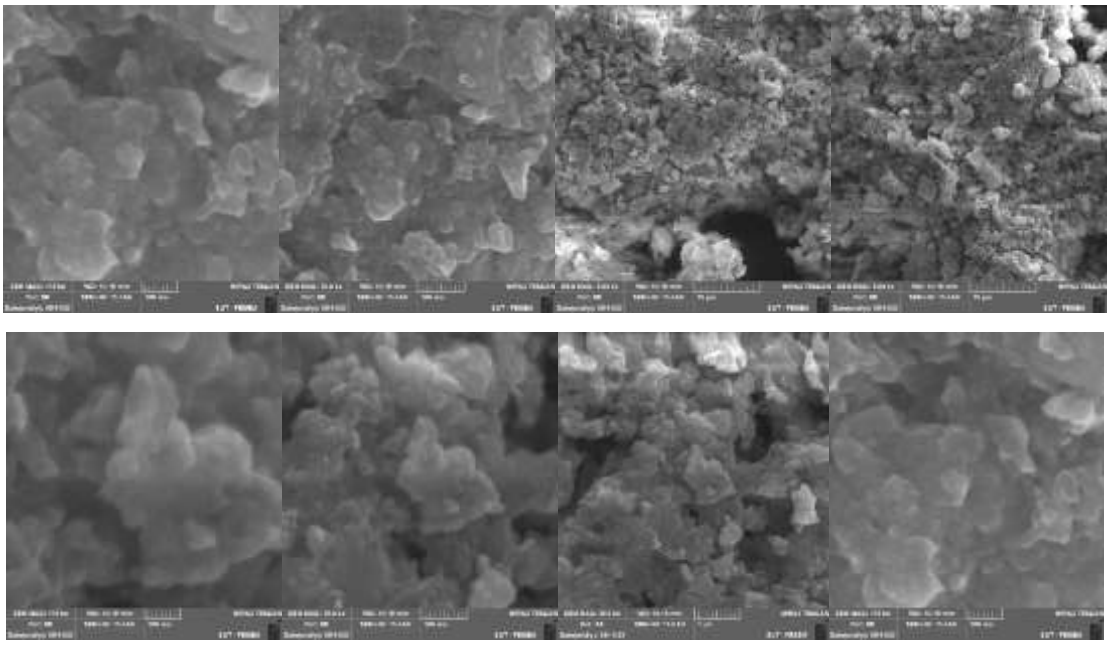

Figure 6-A: FE-SEM examination of low-carbon steels without coated in (1M) HCL acid for (3 hours) and at (50 °C).

Academic Science Journal

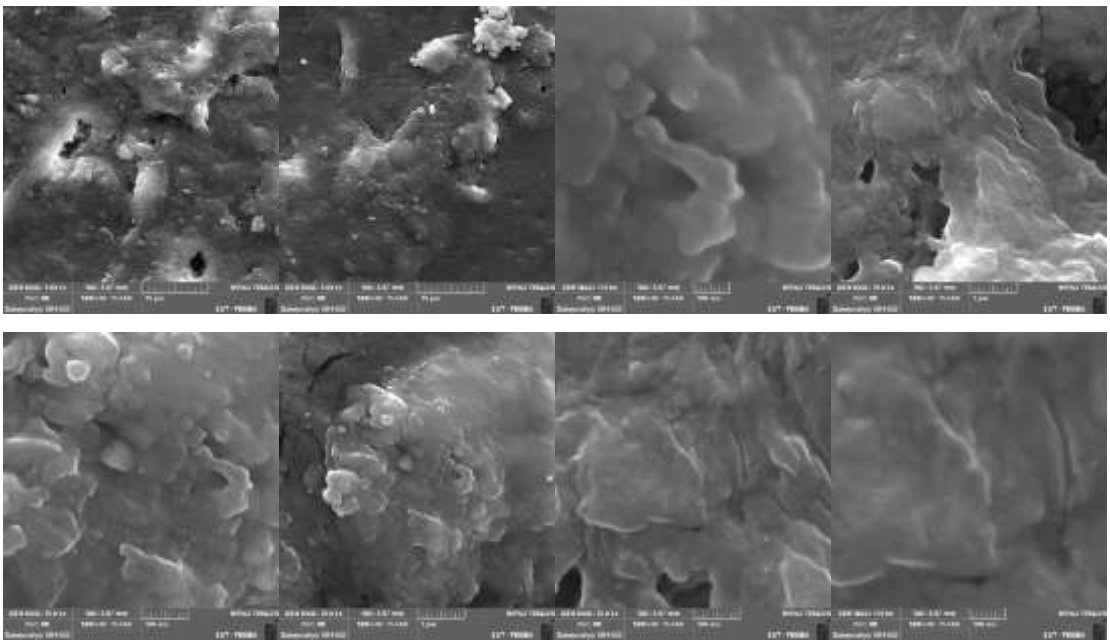

Figure 6-B: FE-SEM examination of low-carbon steels coated with (Epoxy-PANA), after immersing them in (1M) HCL acid for (3 hours) at (50 °C).

Figure 7 represents the FE-SEM examination of the low-carbon steel piece coated with (GO/ Epoxy-PANA) after immersion in (1M) HCL acid for (3 hours) and at (50 °C). From the figure, we notice that the percentage of deformations on the surface of the alloy coated with this material is slightly greater compared to the first case, due to the effect of the coating on acid and heat, where the corrosion results showed that the corrosion rate was (178.1289) and the corrosion prevention efficiency was (97.65207%). However, the coating thus prevents corrosion of low carbon steels.

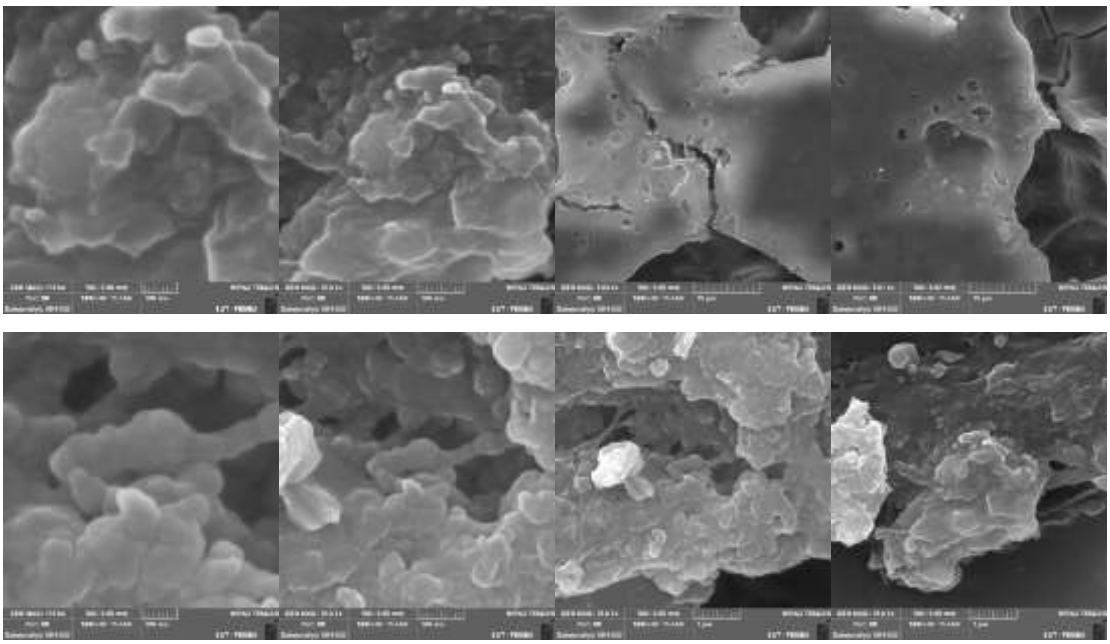

Figure 7: FE-SEM examination of low carbon steels coated with (GO/Epoxy-PANA) after immersing them in (1M) HCL acid for (3 hours) and at (50 °C).

Figure 10 represents the FE-SEM examination of the low-carbon steel piece coated with (GO-10 % WO3/ Epoxy-PANA) of the nanocomposite after immersion in HCL (1M) acid for (3 hours) and temperature (50 degrees). We notice from the figure that some distortions appear on the surface of the alloy coated with this material, and that these distortions and defects are caused by exposure to acid and heat, as the corrosion results showed that the corrosion rate is (79.7433) and the corrosion prevention efficiency is (98.9489%). In doing so, the coating thus prevents corrosion of low-carbon steels.

Academic Science Journal

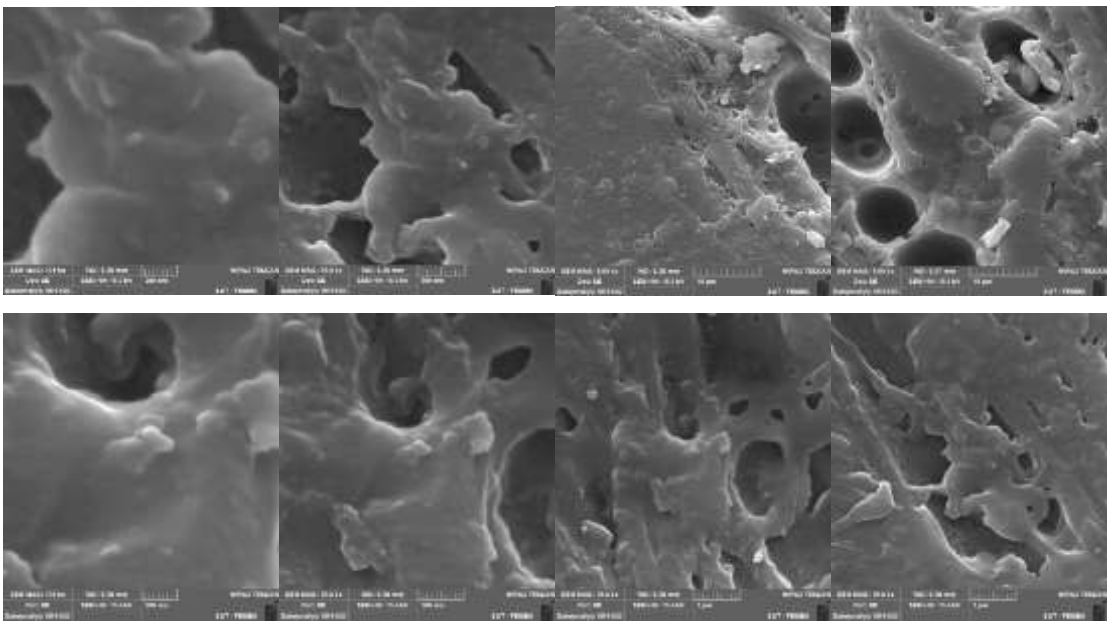

Figure 7: FE-SEM examination of low-carbon steels coated with (GO- 10 % WO3/ Epoxy-PANA) after immersing them in (1M) HCL acid for (3 hours) and at (50 °C).

Study Thermodynamic

The process of creating the polymeric nanocomposite was evaluated through the use of the transition state equation $\ln(C_R) = lnA - \frac{E_a}{RT}$

Whereas, A, Ea, R, and T denote the frequency factor, activation energy, gas constant, and absolute temperature, respectively. The activation energy was determined by utilizing the Arrhenius plot of ln(CR) versus 1/T, with a slope of (-Ea/R) and an intercept of ln(A).

Enthalpy activation (ΔH*) and entropy (ΔS*) were evaluated in this study. The ln(CR/T) values were plotted against (1/T) using Figures (8.A) and (8.B), which allowed for the computation of straight lines. The slopes of these lines were equivalent to (-ΔH*/R), and the intercepts were equal to (ΔS*/R)+ln(R/Nh). The resulting values were tabulated in tables (4) and (5). It was observed that positive ΔH* values indicated an endothermic dissolution process. The literature suggests that exothermic reactions occur during physisorption or chemisorption reactions, while endothermic reactions take place during chemisorption reactions [51-53].

When the value of ΔS* displays negativity, it can be ascribed to the inhibitor molecules being incapable of undergoing hydrolysis in solution and instead forming a cross-linked network on the surface of low carbon steel. This, in turn, culminates in a decline in randomness as the reactants are unable to migrate towards the low carbon steel. On the other hand, in the case of graphene oxide, the inclusion of tungsten oxide percentage tends to result in the inhibitor tungsten oxide molecules becoming more symmetrical on the surface of the sample, thereby leading to a decrease in the entropy value as the percentage of tungsten oxide increases in the graphene oxide. This outcome has been supported by scientific experiments that have established the efficacy of augmenting concentration [54-56]. However, positive values indicate an upswing in the corrosion rate [52-54].

Furthermore, it is observed that the inclusion of (GO - 10 % WO3/ Epoxy-PANA) in the system (as shown in Table 5 with a value of 29.97197 kJ/mol) leads to a reduction in energy to 1.038252 kJ/mol. This empirical evidence reveals that an escalation in inhibitor concentration is associated with a concomitant decrease in activation energy (Ea), thereby signifying a corresponding reduction in the energy barrier for the inhibition reaction. The high activation energy noted in the presence of this substance suggests that the energy of energization undergoes a decline with the progressive augmentation of inhibition (corrosion inhibition). The results from this study show a good agreement with the Linkmuir adsorption temperature. This is confirmed by the presented thermodynamic values, negative standard free energy values signify the spontaneity and endothermic nature of the adsorption process. Furthermore, a reduction in the system's entropy is observed during the process.

Table 4: Enthalpy and entropy of the corrosion process of low carbon steels with different concentrations of (GO - 10 % WO3/ Epoxy-PANA) in (1 M) of hydrochloric acid

Inhibitor	ΔS *(J / mol . K)	Δ H *(kJ / mol)
Epoxy-PANA	-214.0125176	-1.07150832
GO / Epoxy-PANA	-163.4384556	12.3911856
GO - 10 % WO3/ Epoxy-PANA	-214.0158432	-1.47274196
Low carbon steel without inhibitor	-71.33180655	84.752916

Academic Science Journal

Table 5: Corrosion activation energy values for low carbon steels in (1 M) of hydrochloric acid for (GO - 10 % WO3/ Epoxy-PANA)

Inhibitor	Ea (kJ / mol)
Epoxy-PANA	1.439486
GO / Epoxy-PANA	14.90201
GO - 10 % WO3/ Epoxy-PANA	1.038252
Low carbon steel without inhibitor	29.97197

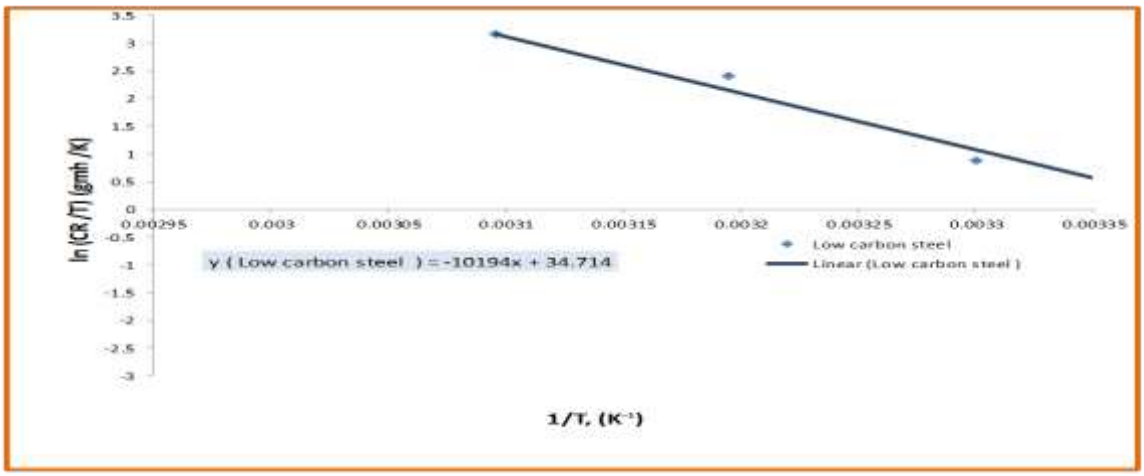

Figure 8-A: Transition state diagram of corrosion of low carbon steel in (1M HCl)

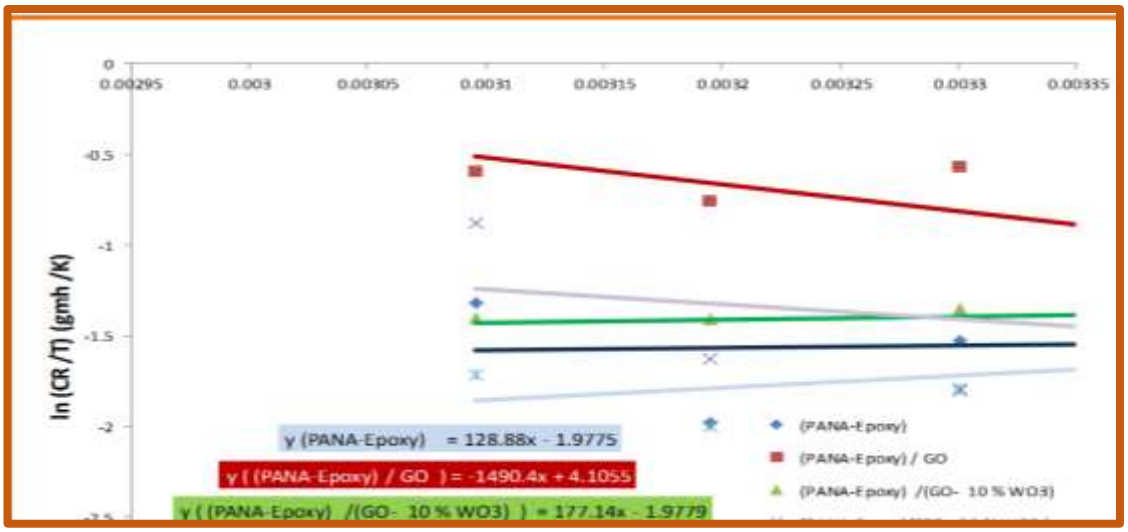

Figure 8-B: Transition state diagram of corrosion of low carbon steel in (1M HCl) in the presence of (GO - 10 % WO3/ Epoxy-PANA).

Conclusions

The (Epoxy-PANA) with (GO - 10 % WO3/ Epoxy-PANA) inhibitor was synthesized and tested as a cor-rosion inhibitor for low carbon steel in hydrochloric acidsolution. FTIR , XRD and SEM analysis were used to diagnosisof (Epoxy-PANA) with (GO - 10 % WO3/ Epoxy-PANA) . The coating prepared from the polymeric nanocomposite (Epoxy-PANA) with (GO - 10 % WO3/ Epoxy-PANA) effectively inhibits the corrosion of low carbon steels in Corrosive solution $1M\ HCl$ and with different temperatures. It can be deduced that the corrosion rate encountered by low carbon steel coated with inhibitor when exposed to a 1M HCl solution is positively correlated with the escalation in temperature. The coatings that were prepared displayed an inhibition efficiency that ranged between 99.00% and 99.9%. It was observed that this inhibition efficiency increased with the difference of the nanocomposites and with the rise in temperature. Conversely, the combined effect of inhibition efficiency increased notably when tungsten oxide was added, while also rising with the increase in temperature. This is attributed to an increase in the percentage of the base component of the paint, which interacts with the surface of the paint, rather than the steel, as the paint serves to protect the steel from corrosion.

References

1. Y. Dong, Y. Yu, J. Xing, B. Xie, M. Zhou, T. Zhao, S. Peng, Hydrophobic polyvinyl butyral/polytetrafluoroethylene composite coating on 5052 aluminum alloy: Preparation, characterization, and anticorrosive properties, Progress in Organic Coatings, 182, 107640(2023)
2. T. Qureshi, G. Wang, S. Mukherjee, M. A. Islam, T. Filleter, C. V. Singh, D. K. Panesar, Graphene-based anti-corrosive coating on steel for reinforced concrete infrastructure applications: Challenges and potential, Construction and Building Materials, 351, 128947(2022)
3. S. I. Daaj, A. N. Abd, Corrosion Inhibition of Mild Steel In (1 M Hcl) Solution Using Plant Extract and The Synergistic Effect of Iodide Ions, Academic Science Journal, 1(2), 120-138(2023)
4. A. N. Abd, E. S. Nasif, Corrosion inhibition of aluminum pure in acidic media using expired drugs aspirin, In: AIP Conference Proceedings, 2475 (1), AIP Publishing, (2023, March)

5. A. A. Khadom, A. N. Abd, N. A. Ahmed, Synergistic effect of iodide ions on the corrosion inhibition of mild steel in 1 M HCl by Cardaria Draba leaf extract, Results in Chemistry, 4, 100668(2022)
6. S. Pourhashem, M. R. Vaezi, A. Rashidi, M. R. Bagherzadeh, Distinctive roles of silane coupling agents on the corrosion inhibition performance of graphene oxide in epoxy coatings, Progress in Organic Coatings, 111, 47-56(2017)
7. H. J. Majidi, A. Mirzaee, S. M. Jafari, M. Amiri, M. Shahrousvand, A. Babaei, Fabrication and characterization of graphene oxide-chitosan-zinc oxide ternary nano-hybrids for the corrosion inhibition of mild steel, International journal of biological macromolecules, 148, 1190-1200(2020)
8. A. Krishnan, B. Joseph, K. M. Bhaskar, M. S. Suma, S. M. A. Shibli, Unfolding the anticorrosive characteristics of TiO2–WO3 mixed oxide reinforced polyaniline composite coated mild steel in alkaline environment, Polymer Composites, 40(6), 2400-2409(2019)
9. M. Gupta, N. Kapoor, A. K. Rai, R. Ameta, S. C. Ameta, Graphene Oxide-Manganese Oxide Composite (GO-MnO2) As a Photocatalyst: A Comparative Study, Journal of Applicable Chemistry, 8(3), 1394-1403(2019)
10. S. Q. Yu, Y. H. Ling, R. G. Wang, J. Zhang, F. Qin, Z. J. Zhang, Constructing superhydrophobic WO3@ TiO2 nanoflake surface beyond amorphous alloy against electrochemical corrosion on iron steel, Applied Surface Science, 436, 527-535(2018)
11. K. C. Yong, Enhancing the Corrosion Inhibition Behaviour of Epoxidized Natural Rubber-Polyaniline Dodecylbenzenesulfonate Blend via the Incorporation of WO3, Polymers and Polymer Composites, 25(2), 135-142(2017)
12. H. Zheng, S. Jiang, Y. Liu, X. Sun, D. Wang, Y. Zhou, L. Zhang, Improved photocathodic protection performance of C-vacancy g-C3N4/GO/WO3 for 304 stainless steel, Journal of Physics and Chemistry of Solids, 160, 110270(2022)
13. H. Norhayati, M. Zuhailimuna, H. Mohd Zobir, M. I. Illyas, M. Azmi, K. Azlan, J. AdilaMohamad, A Brief Review On Recent Graphene Oxide-Based Material Nanoco Mposites: Synthesis And Applications(2016)
14. T. D. Nguyen, A. S. Nguyen, B. A. Tran, K. O. Vu, T. T. Phan, N. Scharnagl, T. X. H. To, Molybdate intercalated hydrotalcite/graphene oxide composite as corrosion inhibitor for carbon steel, Surface and Coatings Technology, 399, 126165(2020)
15. M. Ladan, W. J. Basirun, S. N. Kazi, Polyaniline/graphene oxide/Zn-doped TiO2 nanocomposite coatings for the corrosion protection of carbon steel. Journal of Adhesion Science and Technology, 35(22), 2483-2505(2021)
16. S. Chen, B. Li, R. Xiao, H. Luo, S. Yu, J. He, X. Liao, Design an epoxy coating with TiO2/GO/PANI nanocomposites for enhancing corrosion resistance of Q235 carbon steel, Materials, 14(10), 2629(2021)

17. A. Dey, S. De, A. De, S. K. De, Characterization and dielectric properties of polyaniline–TiO2 nanocomposites, Nanotechnology, 15(9), 1277(2004)
18. F. Branzoi, Z. Pahom, G. Nechifor, Corrosion protection of new composite polymer coating for carbon steel in sulfuric acid medium by electrochemical methods, Journal of Adhesion Science and Technology, 32(21), 2364-2380(2018)
19. J. Aslam, M. Mobin, R. Aslam, F. Ansar, Corrosion protection of low carbon steel by conducting terpolymer nanocomposite coating in 3.5 wt% NaCl solution, Journal of Adhesion Science and Technology, 34(4), 443-460(2020).
20. Z. Spitalsky, D. Tasis, K. Papagelis, C. Galiotis, Carbon nanotube–polymer composites: chemistry, processing, mechanical and electrical properties, Progress in polymer science, 35(3), 357-401(2010).
21. W. Zhang, H. Guo, H. Sun, R. Zeng, Constructing ternary polyaniline-graphene-TiO2 hybrids with enhanced photoelectrochemical performance in photo-generated cathodic protection, Applied Surface Science, 410, 547-556(2017).
22. B. D. Abbass, K. M. Shabeeb, A. K. Hassan, Improve the Corrosion Resistance of the Copper-Zinc Alloy by the Epoxy-WO3 Nanocomposite Coating, Engineering and Technology Journal, 39(11), 1669-1673(2021)
23. N. F. Alheety, A. H. Majeed, M. A. Alheety, Silver nanoparticles anchored 5-methoxy benzimidazol thiomethanol (MBITM): Modulate, characterization and comparative studies on MBITM and Ag-MBITM antibacterial activities, In: Journal of Physics: Conference Series, 1294(5), IOP Publishing, 052026 (2019, September)
24. A. N. Abd, A. H. Al-Agha, M. A. Alheety, Addition of some primary and secondary amines to graphene oxide, and studying their effect on increasing its electrical properties, Baghdad Science Journal, 13(1), 97-112(2016)
25. A. H. Majeed, E. T. B. Al-Tikrity, D. H. Hussain, Dielectric properties of synthesized ternary hybrid nanocomposite embedded in poly (vinyl alcohol) matrix films, Polymers and Polymer Composites, 29(7), 1089-1100(2021)
26. A. A. Khalil, A. F. Shaaban, M. M. Azab, A. A. Mahmoud, A. M. Metwally, Synthesis, characterization and morphology of polyanthranilic acid micro-and nanostructures, Journal of Polymer Research, 20, 1-10(2013)
27. A. A. A.-Z. R. Al-sadi, Study of Polarization Curves for the Carbon Steel (X65-steel) in Acidic Media, University of Qadisiya, (2017)
28. A. A. Khadom, A. N. Abd, N. A. Ahmed, M. M. Kadhim, A. A. Fadhil, Combined influence of iodide ions and Xanthium Strumarium leaves extract as eco-friendly corrosion inhibitor for low-carbon steel in hydrochloric acid, Current Research in Green and Sustainable Chemistry, 5, 100278(2022)
29. F. S. de Souza, A. Spinelli, Caffeic acid as a green corrosion inhibitor for mild steel, Corrosion science, 51(3), 642-649(2009)

30. A. S. A. Nabi, H. M. Ali, Corrosion Inhibition of Carbon steel on Hydrochloric acid Using Zizyphus Spina–Chritisi Extract, Ournal Basrah Researches (Sciences), 35(1), (2009)
31. I. Latif, T. B. Alwan, A. H. Al-Dujaili, Low frequency dielectric study of PAPA-PVA-GR nanocomposites, Nanoscience and Nanotechnology, 2(6), 190-200(2012)
32. A. Dwivedi, S. K. Shukla, P. K. Bharti, N. Gupta, K. K. Saxena, Y. D. Dwivedi, Comparative study of polyanthranilic acid and sulphonated polyaniline on the mild steel corrosion in aqueous hydrochloric acid, Canadian Metallurgical Quarterly, 1-9(2023)
33. H. F. Pang, X. Xiang, Z. J. Li, Y. Q. Fu, X. T. Zu, Hydrothermal synthesis and optical properties of hexagonal tungsten oxide nanocrystals assisted by ammonium tartrate, physica status solidi (a), 209(3), 537-544(2012)
34. A. A. Khan, M. Q. Khan, M. Iqbal, A. Y. Abid, A. R. Khan, Y. Iqbal, M. N. Khan, Facile synthesis of tungsten trioxide 3D architectures by a simple chemical solution route and photodegradation of Rhodamine B: structural, thermal, optical and impedance studies, Journal of Materials Science: Materials in Electronics, 28, 10357-10364(2017)
35. Q. T. Ain, S. H. Haq, A. Alshammari, M. A. Al-Mutlaq, M. N. Anjum, The systemic effect of PEG-nGO-induced oxidative stress in vivo in a rodent model, Beilstein journal of nanotechnology, 10(1), 901-911(2019)
36. A. H. Majeed, D. H. Hussain, E. T. B. Al-Tikrity, M. A. Alheety, Poly (o-Phenylenediamine-GO-TiO2) nanocomposite: modulation, characterization and thermodynamic calculations on its H2 storage capacity, Chemical Data Collections, 28, 100450(2020)
37. P. J. Boruah, R. R. Khanikar, H. Bailung, Synthesis and characterization of oxygen vacancy induced narrow bandgap tungsten oxide (WO 3− x) nanoparticles by plasma discharge in liquid and its photocatalytic activity, Plasma Chemistry and Plasma Processing, 40, 1019-1036(2020)
38. F. Liu, X. Chen, Q. Xia, L. Tian, X. Chen, Ultrathin tungsten oxide nanowires: oleylamine assisted nonhydrolytic growth, oxygen vacancies and good photocatalytic properties, RSC advances, 5(94), 77423-77428(2015)
39. S. Ramkumar, G. Rajarajan, A comparative study of humidity sensing and photocatalytic applications of pure and nickel (Ni)-doped WO 3 thin films, Applied Physics A, 123, 1-8(2017)
40. H. Zhang, M. Yao, L. Bai, W. Xiang, H. Jin, J. Li, F. Yuan, Synthesis of uniform octahedral tungsten trioxide by RF induction thermal plasma and its application in gas sensing, CrystEngComm, 15(7), 1432-1438(2013)

41. N. Kumar, G. K. Sidhu, R. Kumar, Correlation of synthesis parameters to the phase segregation and lattice strain in tungsten oxide nanoparticles, Materials Research Express, 6(7), 075019(2019)
42. R. Al-Gaashani, A. Najjar, Y. Zakaria, S. Mansour, M. A. Atieh, XPS and structural studies of high quality graphene oxide and reduced graphene oxide prepared by different chemical oxidation methods, Ceramics International, 45(11), 14439-14448(2019)
43. M. Kigozi, R. K. Koech, O. Kingsley, I. Ojeaga, E. Tebandeke, G. N. Kasozi, A. P. Onwualu, Synthesis and characterization of graphene oxide from locally mined graphite flakes and its supercapacitor applications, Results in Materials, 7, 100113(2020)
44. S. Aodah, N. Bano, I. Hussain, M. S. AlSalhi, Quantitative analysis of the Schottky interface of reduced graphene oxide Schottky diodes, Materials Research Express, 7(9), 095007(2020)
45. S. Hoseinzadeh, R. Ghasemiasl, A. Bahari, A. H. Ramezani, The injection of Ag nanoparticles on surface of WO 3 thin film: enhanced electrochromic coloration efficiency and switching response, Journal of Materials Science: Materials in Electronics, 28, 14855-14863(2017)
46. D. D. Nguyen, D. V. Dang, D. C. Nguyen, Hydrothermal synthesis and NH3 gas sensing property of WO3 nanorods at low temperature, Advances in Natural Sciences: Nanoscience and Nanotechnology, 6(3), 035006(2015)
47. P. S. Kolhe, P. S. Shirke, N. Maiti, M. A. More, K. M. Sonawane, Facile hydrothermal synthesis of wO 3 Nanoconifer thin film: Multifunctional behavior for gas sensing and field emission applications, Journal of Inorganic and Organometallic Polymers and Materials, 29, 41-48(2019)
48. N. F. Alheety, L. A. Mohammed, A. H. Majeed, A. Aydin, K. D. Ahmed, M. A. Alheety, S. Dohare, Antiproliferative and antimicrobial studies of novel organic-inorganic nanohybrids of ethyl 2-((5-methoxy-1H-benzo [d] imidazol-2-yl) thio) acetate (EMBIA) with TiO2 and ZnO, Journal of Molecular Structure, 1274, 134489(2023)
49. L. A. Adnan, N. F. Alheety, A. H. Majeed, M. A. Alheety, H. Akbaş, Novel organic-inorganic nanohybrids (MnO2 and Ag nanoparticles functionalized 5-methoxy-2-mercaptobenzimidazole): one step synthesis and characterization, Materials Today: Proceedings, 42, 2700-2705 (2021)
50. M. A. Alheety, A. H. Majeed, A. H. Ali, L. A. Mohammed, A. Destagul, Destagul, P. K. Singh, Synthesis and characterization of eggshell membrane polymer-TiO2 nanocomposite for newly synthesized ionic liquid release, Journal of the Iranian Chemical Society, 19(9), 4005-4015(2022)

51. S. I. Daaj, A. N. Abd, Corrosion Inhibition of Mild Steel In (1 M Hcl) Solution Using Plant Extract and The Synergistic Effect of Iodide Ions, Academic Science Journal, 1(2), 120-138(2023)
52. I. El Ouali, B. Hammouti, A. Aouniti, Y. Ramli, M. Azougagh, E. M. Essassi, M. Bouachrine, Thermodynamic characterisation of steel corrosion in HCl in the presence of 2-phenylthieno (3, 2-b) quinoxaline, J. Mater. Environ. Sci, 1(1), 1-8(2010)
53. R. J. Jadaa, A. N. Abd, A. A. Khadom, Polyacrylamide as a corrosion inhibitor for mild steel in 2 M phosphoric acid: Experimental and theoretical studies, Chemical Papers, 75, 5375-5386(2021)
54. X. H. Chen, C. S. Chen, H. N. Xiao, F. Q. Cheng, G. Zhang, G. J. Yi, Corrosion behavior of carbon nanotubes–Ni composite coating, Surface and Coatings Technology, 191(2-3), 351-356(2005)
55. A. A. Khadom, A. N. Abd, N. A. Ahmed, Xanthium strumarium leaves extracts as a friendly corrosion inhibitor of low carbon steel in hydrochloric acid: Kinetics and mathematical studies, south african journal of chemical engineering, 25, 13-21(2018)
56. A. A. Khadom, A. N. Abd, N. A. Ahmed, Potassium iodide as a corrosion inhibitor of mild steel in hydrochloric acid: kinetics and mathematical studies, Journal of Bio-and Tribo-Corrosion, 4(2), 17(2018)